Prototype of a new Transverse-Flux Permanent Magnet (TFPM) Machine with Toothed Rotor

M. R. Dubois, H. Polinder and J.A. Ferreira
Laboratory of Electrical Power Processing
Delft University of Technology
Mekelweg 4, 2628 CD Delft, The Netherlands,
phone: +31 15 278 6259 – fax: +31 15 278 29 68 – e-mail: m.dubois@its.tudelft.nl,
h.polinder@its.tudelft.nl, j.a.ferreira@its.tudelft.nl,

***Abstract*—Transverse-Flux Permanent Magnet machines provide substantial savings in the amount of active material. The Transverse-Flux Permanent Magnet Machine with Toothed Rotor also improves the manufacturability of the rotor parts. An analytical model is developed, based on equivalent magnetic circuits and lumped reluctances. An optimal machine design is derived, and a prototype is built and described.**

1. Introduction

The principle of Transverse-Flux Permanent Magnet (TFPM) machines has been discussed in a number of publications [1]-[3]. TFPM machines mostly find their applications where high torque and low-to-medium rotational speed are required. The high torque/mass ratio makes TFPM machines an attractive solution to reduce the cost of active material in low-speed direct-drive applications, like wind turbine generators. However, if cost-competitiveness is an issue, not only TFPM machines must have a low mass of active material, but also must they be easy to produce.

In [4], a TFPM machine with toothed rotor is derived. In this paper, a rotating machine is built, which uses the TFPM geometry with toothed rotor. The design is optimized for lowest cost/torque. The optimization is based on analytical models presented in the paper.

2. TFPM Machine with toothed rotor

In [4], the TFPM machine with toothed rotor was described. The resulting machine configuration is shown in fig. 1 and fig. 2.

The TFPM machine with toothed rotor has the following characteristics: a) permanent magnets in flux concentration, b) stator cores built with laminated steel, c) single-sided stator, d) location of each magnet in the rotor is independent from the sum of mechanical tolerances due to the other rotor pieces, e) magnet and flux concentrators can be built and inserted in the rotor structure using an automated process.

A. Production of flux–concentrating TFPM machines

Different authors have emphasized the advantages of TFPM machines, but also the difficulties of building them. If TFPM machines are to be produced in large quantities, the manufacturing process should be carefully investigated.

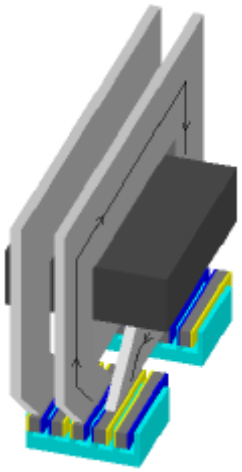

Fig.1. Five (5) poles of the TFPM machine with toothed rotor (linear version).

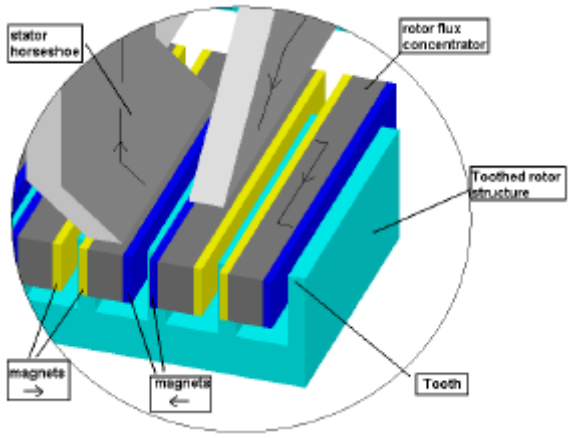

Fig.2. Close-up on the TFPM machine with toothed rotor.

The stator winding of most TFPM machines is very simple. However, other parts of past TFPM machines present important production difficulties. In flux-concentrating configurations, the rotor construction can be substantially improved by using a toothed rotor structure. Such structure can be made from a stack of laminations, where each lamination is stamped individually from a die of alternating teeth and slots. This kind of arrangement is also comparable to the stator of conventional synchronous machines. The toothed laminations are shown in fig. 3.

Each rotor pole can be assembled independently, outside the machine. Then each sub-assembly can be inserted into the toothed rotor structure, as shown in fig. 3.

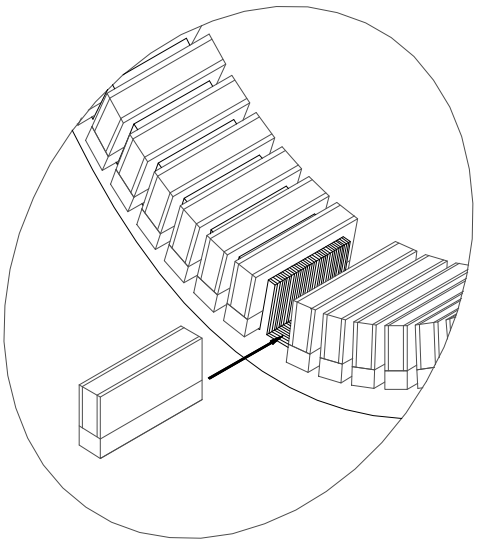

Fig.3. One row of the laminated rotor structure (stator is not shown).

For each pole, rotor sub-assemblies are formed by two magnets with opposite directions of magnetization, one flux concentrator and one insulating block. The insulating block prevents short-circuiting the magnet fluxes through the toothed structure. Also, the insulating block and the slot may be designed with a trapezoidal shape, offering a natural attachment for the rotor poles to the slots.

B. Use of laminations in the stator

The TFPM machine with toothed rotor allows laminated steel to be used in the stator parts, due to the planar flux circulation. Laminated steel gives better performances than powdered iron , as long as the magnetic flux travels parallel to the lamination planes. A very important difference between powdered iron and laminated steel is the specific iron losses. They are about seven (7) times lower in 0.35-mm thick laminated electric steel at 400 Hz [4] in the case of planar flux circulation. This point is of utmost importance in TFPM machines, where pole pitches are short and consequently electrical frequencies are rather high.

In the unaligned position, the net flux linking the stator winding will be zero at no-load. However, the rotor poles will exchange flux through the stator core, in a direction perpendicular to the plane of the steel laminations. This will create higher losses, which may favor powdered iron for this particular case. This effect was not considered in the following analysis, and is open for further investigation.

C. Reducing leakage between the stator cores

One significant problem in single-sided TFPM stators is the stator leakage flux between the stator horseshoe and the core forming the return path. In the proposed structure, the problem is dealt with, by forming the return path into a trapezium and by shaping the horseshoe core with a leg and a foot. This reduces the area of flux leakage between the two stator cores.

The stator leakage flux can be reduced further, if the flux concentrators and magnets are made slightly longer than the rotor stack, as shown in fig. 2. The length of the stator foot is made a little shorter than the flux concentrator, thus reducing the leakage area between the stator horseshoe and the stator trapezium. In that case, the flux concentrators are also used to carry the flux in the axial direction.

It must be noted that the toothed rotor structure has formed an additional leakage path between the stator horseshoe and the trapezoidal flux return when the stator cores face the teeth. This leakage path can be partly eliminated by reducing the rotor tooth height. A factor 3-4 between the air gap and the stator-tooth distance is generally sufficient to reduce the tooth leakage flux to negligible levels.

3. Modeling of the TFPM Machine with toothed rotor

A linear actuator was built in [4], which demonstrates the ability of the TFPM machine with toothed rotor to produce tangential forces. However, this linear actuator was not an optimized design.

To optimize the design performance, an analytical model is developed in this section. From the analytical model, an optimization program can be developed and optimal designs may be obtained with less computational time than with 3-D finite element analysis methods (FEM).

The TFPM machine is essentially a single-phase machine. It is possible to turn it into a three-phase machine, by stacking three TFPM machines, and shifting their rotors by 120^o. The torque of a single-phase machine with salient poles can be expressed as:

$$T \cong \frac{EI}{\Omega}\cos d + \frac{pI^2 f(L_u - L_a)}{2\Omega}\sin 2d \qquad (1)$$

where the no-load losses are neglected and where the no-load voltage and phase current are assumed as sinusoidal. The stator inductance is assumed as varying sinusoidally with the electrical angle, between two values L_a and L_u.

Expression (1) is written as a function of the global electrical quantities E, I, L, f, Ω. We can also derive a similar expression for T, expressed on a per pole-pair basis:

$$T = \frac{p^2}{2}F_s\left[\Phi_{pnl}\cos d + \frac{F_s}{4}\left(\frac{1}{R_{up}} - \frac{1}{R_{ap}}\right)\sin 2d\right] \qquad (2)$$

A. Calculation of F_{pnl} and R_{ap}

In TFPM machines, the pole pitch is generally short. This makes the flux calculation difficult, due to the different leakage paths directed in all 3 dimensions. The leakage flux paths and main paths are shown in fig. 4 and fig. 5.

An equivalent magnetic circuit may be derived from the leakage paths and main paths identified in fig. 4 and fig. 5. This equivalent circuit is shown in fig. 6. The values of Φ_{pnl} and R_{ap} are obtained by solving the magnetic circuit of fig. 6, giving expressions (3) and (4).

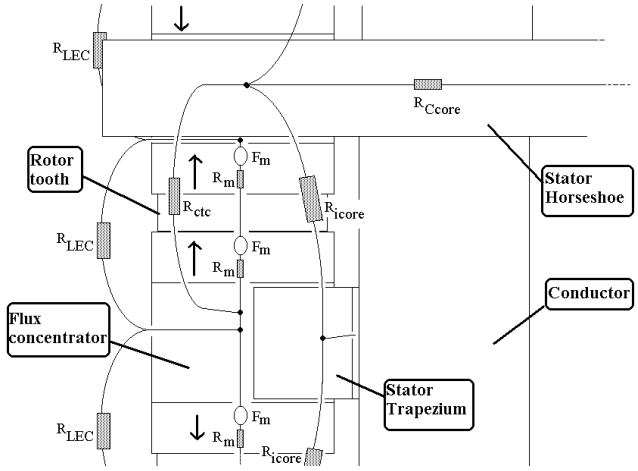

Fig. 4. Leakage paths represented as lumped reluctances in the aligned position (top view).

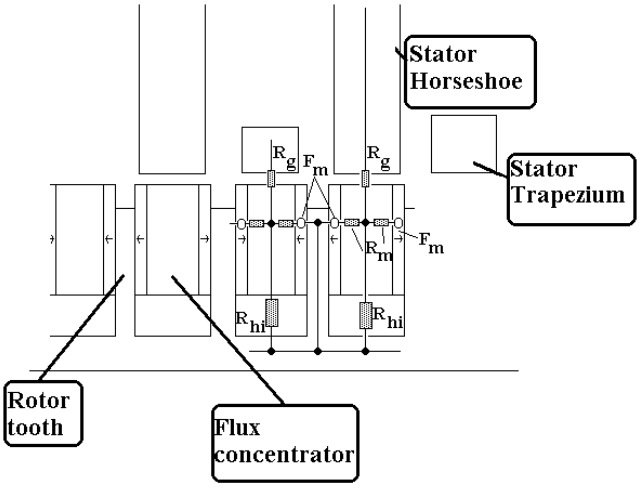

Fig. 5. Leakage paths represented as lumped reluctances in the aligned position (side view).

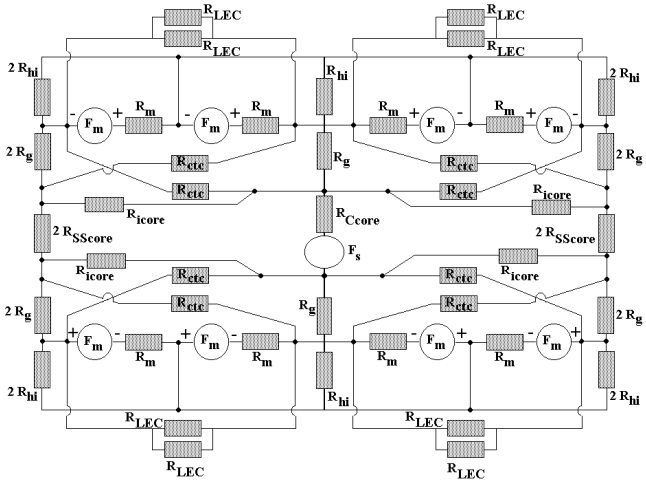

Fig. 6. Magnetic circuit in the aligned position, used for the calculation of F_{pnl} and R_{ap}.

$$\Phi_{pnl}=\frac{F_m\left(R_{ctc}-2R_g\right)}{R_gR_m+R_{ctc}\left(2\frac{R_gR_m}{R_{eq}}+R_g+\frac{R_m}{2}\right)+R_{stator}\left(\frac{R_gR_m}{R_{eq}}+\frac{R_{ctc}R_m}{2R_{eq}}+\frac{R_g}{2}+R_m+\frac{R_{ctc}}{4}\right)} \quad (3)$$

where

$$R_{ap}=\frac{R_{eq3}R_{icore}}{R_{eq3}+R_{icore}}+R_{SScore}+R_{Ccore} \quad (4)$$

$$R_{stator}=R_{Ccore}+R_{SScore} \quad (5)$$

$$R_{eq}=\frac{2R_{hi}R_{LEC}}{4R_{hi}+\frac{R_{LEC}}{2}} \quad (6)$$

$$R_{eq3}=R_{T12}+\frac{(R_{T2}+R_{ctc})(R_{T1}+2R_g)}{R_{T2}+R_{ctc}+R_{T1}+2R_g} \quad (7)$$

$$R_{T1}=\frac{R_{ctc}R_{eq2}}{R_{ctc}+R_{eq2}+2R_g} \quad (8)$$

$$R_{T2}=\frac{2R_gR_{eq2}}{R_{ctc}+R_{eq2}+2R_g} \quad (9)$$

$$R_{T12}=\frac{2R_gR_{ctc}}{R_{ctc}+R_{eq2}+2R_g} \quad (10)$$

$$R_{eq2}=\frac{4R_{hi}R_mR_{LEC}}{8R_mR_{hi}+2R_{hi}R_{LEC}+R_mR_{LEC}} \quad (11)$$

B. Calculation of R_{up}

The magnetic circuit in the unaligned position is defined from the lumped reluctances shown in fig. 7. The equivalent magnetic circuit in the unaligned position is shown in fig. 8. The circuit of fig. 8 can be solved, giving the reluctance R_{up} as:

$$R_{ap}=\frac{R_AR_B}{R_A+R_B}+R_{SScore}+R_{Ccore} \quad (12)$$

where

$$R_A=\frac{4R_{icore}R_t\left(1+\frac{R_t}{R_{hi}}+2\frac{R_t}{R_m}\right)}{R_{icore}+4R_t\left(1+\frac{R_t}{R_{hi}}+2\frac{R_t}{R_m}\right)} \quad (13)$$

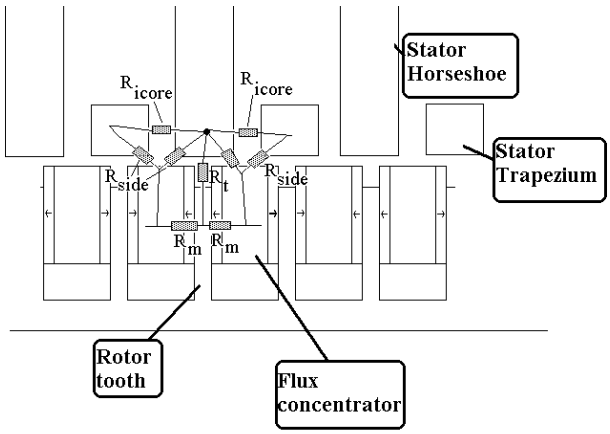

Fig. 7 Leakage paths represented as lumped reluctances in the unaligned position (side view).

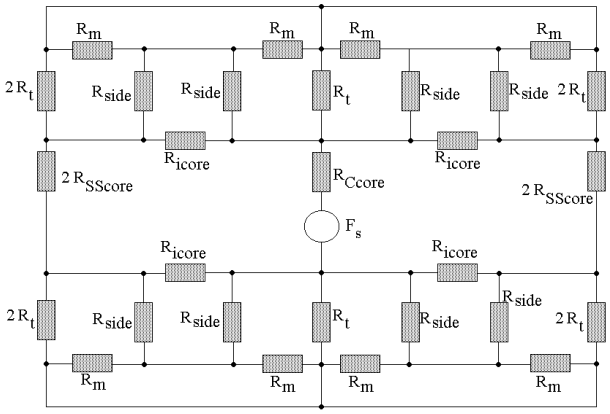

Fig. 8. Magnetic circuit used for the calculation of R_{up}.

and where

$$R_B = \frac{4R_{side}\left(R_t + \dfrac{R_{hi}R_m}{2R_{hi}+R_m}\right)}{R_{side} + 2R_t + 2\dfrac{R_{hi}R_m}{2R_{hi}+R_m}} \tag{14}$$

C. Calculation of the lumped reluctances

To calculate the value of the lumped reluctances R_m, R_{Ccore}, R_{SScore}, R_{LEC}, R_{ctc}, R_g, R_{side}, R_t, R_{icore}, R_{hi}, and the mmf F_m, we use (15)-(23). Equations (20)-(23) are derived from linear regressions performed on a collection of reluctances calculated from a high number of 3-D finite element computations.

$$R_t = \frac{h_{ru}+g}{\mu_0 w_{rc1} l_f} \tag{15}$$

$$F_m = \frac{h_m B_r}{\mu_0 \mu_{rm}} \tag{16}$$

$$R_m = \frac{h_m}{\mu_0 \mu_{rm} l_{rt1}(w_m - h_{ru})} \tag{17}$$

$$R_{Ccore} = \frac{l_{sw} + 2h_{sw} + (2\sqrt{2}+1)l_f}{\mu_0 \mu_{rFe} w_{sc} l_f} \tag{18}$$

$$R_{SScore} \cong \frac{l_{sw} + \sqrt{2}l_f - 2l_{rt1}}{\mu_0 \mu_{rFe} w_{sc} l_f} \tag{19}$$

$$R_g = \frac{g}{\mu_0 l_f w_{rc2}}\left[1.3 - 0.6\frac{w_{sc}}{w_{rc2}} + 0.2\frac{w_{sc}^2}{w_{rc2}^2} + 0.03\frac{w_{rc2}}{g} - 6.4\times10^{-4}\frac{w_{rc2}^2}{g^2} - 2.3\frac{g}{l_f} + 3.8\frac{g^2}{l_f^2}\right] \tag{20}$$

$$R_{side} = \frac{g}{\mu_0 l_f w_{rc2}}\left[1.6 + 0.49\frac{d}{g} - 0.93\frac{d}{w_{rc2}} - 1.04\frac{w_{sc}}{w_{rc2}} + 0.16\frac{w_{sc}}{g}\right] \tag{21}$$

$$R_{icore} = \frac{t_p - w_{sc}}{\mu_0 l_f^2}\left(8.1 + 9.7\frac{t_p - w_{sc}}{l_f} - 1.2\frac{(t_p - w_{sc})^2}{l_f^2} - 15\sqrt{\frac{t_p - w_{sc}}{l_f}} - 1.9\frac{l_f^2}{l_{rt1}^2}\right) \tag{22}$$

$$R_{hi} = \frac{h_{ri}}{\mu_0 l_{rt1} w_{rc2}}\left(-0.03 + 0.3\frac{2h_m + w_{rc2}}{h_{ri}} - 0.03\frac{(2h_m + w_{rc2})^2}{h_{ri}^2}\right) \tag{23}$$

D. Calculation of F_{smax}

The torque of the TFPM machine can be predicted from (2), if the magnetomotive force F_s fed into the stator winding is known. Since we are interested by the maximum available torque, we need to find F_{smax}, the maximum value of F_s. F_{smax} is determined from the expression of the flux $\Phi_{ps}(t)$ created by the armature reaction in the core of a salient TFPM machine, fed with a sinusoidal current.

$$\Phi_{ps}(t) = \frac{F_s}{4}\left(\sin d\left[\left(\frac{1}{R_{up}} + \frac{3}{R_{ap}}\right)\cos wt + \left(\frac{1}{R_{up}} - \frac{1}{R_{ap}}\right)\cos 3wt\right]\right) + \ldots$$

$$\ldots\frac{F_s}{4}\left(\cos d\left[\left(\frac{1}{R_{up}} + \frac{3}{R_{ap}}\right)\sin wt + \left(\frac{1}{R_{up}} - \frac{1}{R_{ap}}\right)\sin 3wt\right]\right) \tag{24}$$

The total flux flowing in one stator core of the TFPM machine is the sum of the no-load flux per pole $\Phi_{pnl}(t)$ and the flux $\Phi_{ps}(t)$ created by the armature reaction:

$$\Phi_{ptot}(t) = \Phi_{ps}(t) + \Phi_{pnl}\cos(v\,t - p) \tag{25}$$

The value of F_{smax} is limited by the saturation flux density B_{Fesat} in the stator core. The saturation flux is defined as:

$$\Phi_{psat} = B_{Fesat} w_{sc} l_f \tag{26}$$

To obtain F_{smax}, we vary $w\,t$ by software between *0* and *2p*, and set Φ_{ptot} to its saturation flux Φ_{psat} defined by (26). For each value of $w\,t$, a value for F_s is obtained by using (24) and (25). The lowest value of F_s must be retained, provided that all other values will saturate the stator core. This is the value retained as F_{smax}.

4. Optimization and design of a TFPM machine with toothed rotor

To identify the most suitable design, a computer program has been developed. The program uses the model described in the last section to predict the machine torque for each set of geometrical parameters. The program allows these geometrical parameters to vary within a certain range and identify the optimal design. In this case, the optimization criterion was cost/torque, where steel laminations, copper and powdered iron had been given a specific cost of 6 Euros/kg, and 40 Euros/kg for Nd-Fe-B permanent magnets.

For an airgap diameter of 46 cm and an airgap thickness of 1 mm, the optimal design has the following characteristics: width of flux concentrator = 6 mm, magnet thickness = 2 mm, thickness of insulating block = 5 mm,

length of rotor poles = 48 mm, length of stator foot = 40 mm, height of magnets and flux concentrators (in the radial direction) = 12 mm, number of conductor turns = 27.

Using the optimization program, the best performances were obtained with large stator core cross-sections. This allows higher ampère-turns in the stator winding before saturating the stator cores. However, this also leads to high values of per-unit reactance. For example, a stator core width w_{sc} of 10 mm would give the best torque performance (1100 Nm), but the power factor would be low due to a per-unit reactance of 2.6. If w_{sc} is decreased to 4 mm, the per-unit reactance is decreased to lower values (1.1), at the expense of a torque performance 60% lower (468 Nm). In the design, a compromise was made between high torque performance and high power factor, by using a w_{sc} of 8 mm.

A second compromise had to be made, concerning the tooth width w_{rc1} in the rotor toothed structure. In general, the shorter the tooth width, the higher the number of poles, and the higher the torque value. For this design, the torque/mass performance could be improved by 10% with a tooth width of 2 instead of 4 mm. However, for structural reasons, a tooth width of 4 mm was chosen. With a tooth width of 4 mm, the pole pitch t_p is 14 mm, and the number of pole pairs p is 52 per phase. The mass of active material is 68 kg/phase, and the nominal torque rating is 1000 Nm/phase. The maximum mmf F_{smax} is 2746 A-t, the no-load flux Φ_{pnl} is 267 μWb/pole pair, the reluctances seen by the winding in the aligned (R_{ap}) and unaligned (R_{up}) positions are respectively 5.4 A-t/μWb and 4.6 A-t/μWb per pole pair.

In all calculations, the following values were used: J = 4.0 A/mm^2, k_{sfill} = 0.5, B_r = 1.10 T, μ_{rFe} = 2000, μ_{rm} = 1.09, B_{FEsat} = 1.8 T, N = 100 rpm.

A. Sensitivity of machine performances to air gap thickness

If the geometry described above is used and only the air gap thickness is allowed to vary, fig. 9 shows the decrease of nominal torque and increase in per unit reactance for an increasing air gap thickness, as predicted from the model. As pointed out in [5], the performances of TFPM machines with flux-concentration are very much dependent upon the airgap thickness. This is also the case with the TFPM machine with toothed rotor. Consequently, an airgap of 1 mm was used in the prototype described in the next section.

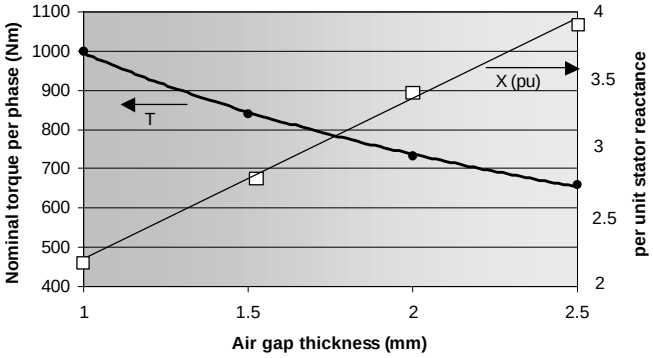

Fig. 9. Sensitivity of machine performance to airgap thickness (square = p.u. stator reactance, dot = nominal torque).

5. Experiments on a rotating TFPM machine with toothed rotor

The TFPM machine with toothed rotor was built, according to the design specifications obtained in the last section. Fig. 10 shows the stator of the 3-phase machine, before the winding process. As can be seen from fig. 10, the winding process is easy. Fig. 11 shows the machine with the stator fully mounted, and only one rotor phase mounted.

Fig. 10. Stator cores before winding. Rotor and trapeziums not mounted.

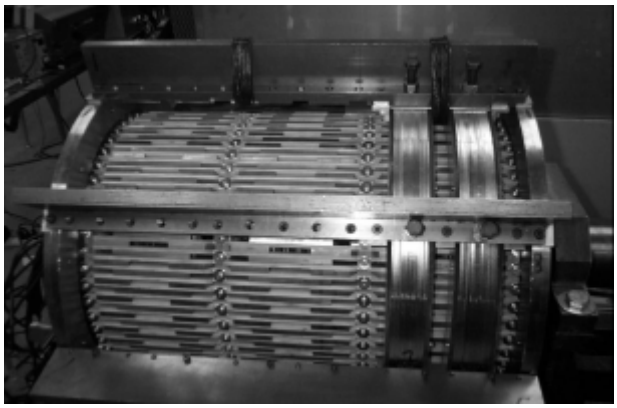

Fig. 11. Prototype of the TFPM machine with toothed rotor. Three stator phases and one rotor phase are shown.

Experiments could be carried out on one phase used as a generator. The no-load waveform is shown in fig. 12.

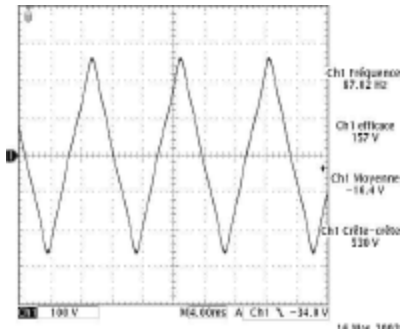

Fig. 12. No-load voltage across one stator phase (N = 100 rpm). 100 V/div.

The no-load flux per pole pair Φ_{pnl} measured from fig. 12 is 272 μWb in the aligned position. The model predicted a value of 267 μWb, which shows very good agreement with measurements. Then, the machine was loaded with a resistor in series with a capacitor, to compensate the large stator reactance. Fig. 13 shows the voltage and current waveforms under loaded conditions.

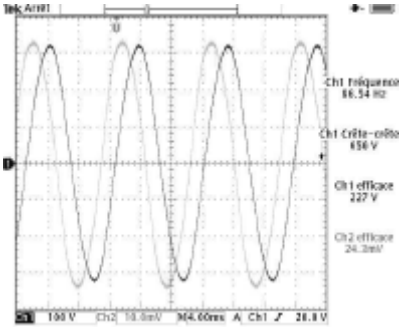

Fig. 13. Voltage and current waveforms with a load of C= 448 uF in series with R = 2.2 Ohms (N = 100 rpm). 100 V/div, 20 A/div.

The voltage and current waveforms are more sinusoidal under loaded conditions than the no-load voltage of fig. 12. The maximum torque extracted from the machine was limited to 720 Nm, due to the non-linearity of the stator inductance. This limits the range where useful compensation can be achieved with capacitors. At high current values, the stator inductance decreases very fast due to the stator B(H) curve, and the load impedance becomes too high to extract higher power from the machine. In further experiments, the capacitive load will be replaced by a voltage-source inverter, which will enable a more flexible load control.

6. Conclusion

The TFPM machine with toothed rotor offers improved rotor construction. A model based on lumped reluctances and equivalent magnetic circuit was developed, which allows fast optimization. The lumped reluctances are approximations derived from linear regression analysis. Based on the equivalent magnetic circuit, the model described in this paper enables approximating the machine nominal torque. A TFPM machine with toothed rotor was built, which geometrical parameters were derived from the model-based optimization. The no-load flux could be successfully predicted with the model. Under load conditions, the peak torque could not be tested with capacitors and resistors. Only 72% of the maximum torque could be tested with the linear loads. A voltage-source inverter is required in order to push the stator core into the non-linear region of its B(H) curve, and then extract the maximum power.

Acknowledgement

The authors want to thank DU-WIND (The Netherlands) and the FCAR (Québec, Canada) for financially supporting Mr. Dubois's research. Also, the authors want to thank Eocycle Technologies Inc. for their financial support to the experimental part of this research.

The concept of TFPM machine with toothed rotor is protected by an international patent application.

References

[1] H. Weh, "Permanentmagneterregte Synchronmaschinen hoher Kraftdichte nach dem Transversalflusskonzept," *etzArchiv*, vol. 10, pp. 143-149, 1988.

[2] G. H. Pajooman, Performance Assessment and Design Optimisation of VRPM (Transverse Flux) Machines by Finite Element Computation, Ph.D. dissertation, Dept. Elect. Eng., Univ. Southampton (1997), England.

[3] C.P. Maddison, B.C. Mecrow and A.G. Jack, "Claw Pole Geometries for High Performance Transverse Flux Machines", in *Proc. ICEM1998*, Vol. 1, pp. 340-345.

[4] M.R. Dubois, H. Polinder and J.A. Ferreira, "Transverse-Flux Permanent Magnet (TFPM) Machine with Toothed Rotor", in *Proc. IEE Conf. Pow. Electr. Mach.&Drives 2002*, pp. 309-314.

[5] M.R. Dubois, H. Polinder and J.A. Ferreira, "Influence of Air Gap Thickness in Transverse Flux Permanent Magnet (TFPM) Generators for Wind Turbine Application", in *Proc. IEEE Young Researchers Symposium in Elec. Pow. Eng. 2002,* Leuven, Belgium.

Nomenclature

B_{Fesat} = saturation flux density of laminated steel, B_r ,= remanent flux density of permanent magnets, C = load compensating capacitance value (in series with R), d = overlap distance between stator core and flux concentrator, E = rms no-load voltage, f = electrical frequency in Hz, F_m = PM equivalent magnetomotive force (mmf), F_s = amplitude of the stator magnetomotive force, F_{smax} = maximum value of F_s obtained at saturation, g = air gap thickness, h_m = magnet thickness, h_{ri} = thickness of insulating block between flux concentrator and slot bottom in the radial direction, h_{ru} = distance between the tip of the rotor tooth and the flux concentrator in the radial direction, h_{sw} = height of stator winding in radial direction , I = rms nominal phase current, J = rms current density in the conductors , k_{sfill} = winding filling factor, l_f = length of stator foot in axial direction, l_{rt1} = length of flux concentrator in axial direction, l_{sw} = width of stator winding in axial direction , L_a = stator inductance for rotor in aligned position, L_u = stator inductance for rotor in unaligned position, N = machine rotational speed in rpm, p = number of pole pairs, P_{mech} = mechanical power on the machine shaft, R = load resistance value, R_m = PM recoil reluctance, R_g = air gap reluctance, R_{hi} = reluctance of insulating block between flux concentrator and slot bottom for one rotor pole, R_{side} = reluctance of leakage path between stator core and rotor flux concentrator in unaligned position, R_{up} = reluctance per pole pair seen by the stator conductors in unaligned position R_{ap} = reluctance per pole pair seen by the stator conductors in aligned position, R_{Ccore} = reluctance of stator horseshoe steel core, R_{SScore} = reluctance of stator trapezium steel core, R_{icore} = reluctance of leakage path between stator core and stator trapezium core, R_{LEC} = reluctance of leakage path between two adjacent flux concentrators in the rotor, R_{ctc} = reluctance of leakage path between stator core and adjacent flux concentrator in aligned position, R_t = reluctance between stator core and rotor tooth in unaligned position, T = average continuous mechanical torque, w_m = magnet width in the circumferential direction , w_{sc} = stator core width, w_{rc1} = width of rotor tooth in the circumferential direction, w_{rc2} = width of flux concentrators (rotor) in the circumferential direction, δ = phase angle between no-load voltage and phase current, Φ_{pnl} = no-load flux in the aligned position in one pole of the stator core, Φ_{ps} = flux component created by the armature reaction in the stator core, Φ_{psat} = saturation flux in one pole of the stator core, Φ_{ptot} = sum of no-load flux and armature reaction in one pole of the stator core, μ_{rm} = recoil relative permeability of permanent magnets, μ_{rFe} = relative permeability of laminated steel, τ_p = pole pitch, ω = electrical angular frequency in rad/s, Ω = machine angular rotational speed in rad/s